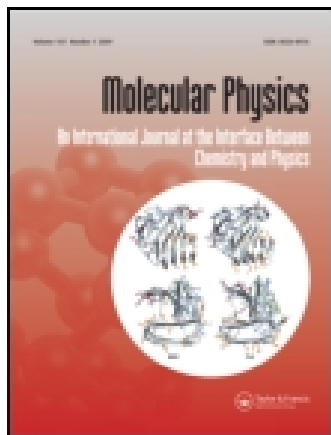


This article was downloaded by: [North Dakota State University]

On: 14 October 2014, At: 00:06

Publisher: Taylor & Francis

Informa Ltd Registered in England and Wales Registered Number: 1072954 Registered office: Mortimer House, 37-41 Mortimer Street, London W1T 3JH, UK



Molecular Physics: An International Journal at the Interface Between Chemistry and Physics

Publication details, including instructions for authors and subscription information:

<http://www.tandfonline.com/loi/tmph20>

Quasi-2D and prewetting transitions of square-well fluids on a square-well substrate

Ashim K. Saha^a, Satya Pal Singh^a, Jayant K. Singh^a & Sang Kyu Kwak^b

^a Department of Chemical Engineering, Indian Institute of Technology Kanpur, Kanpur, India 208016

^b Division of Chemical and Biomolecular Engineering, School of Chemical and Biomedical Engineering, Nanyang Technological University, Singapore 637459

Published online: 28 Sep 2009.

To cite this article: Ashim K. Saha, Satya Pal Singh, Jayant K. Singh & Sang Kyu Kwak (2009) Quasi-2D and prewetting transitions of square-well fluids on a square-well substrate, *Molecular Physics: An International Journal at the Interface Between Chemistry and Physics*, 107:20, 2189-2200, DOI: [10.1080/00268970903222165](https://doi.org/10.1080/00268970903222165)

To link to this article: <http://dx.doi.org/10.1080/00268970903222165>

PLEASE SCROLL DOWN FOR ARTICLE

Taylor & Francis makes every effort to ensure the accuracy of all the information (the "Content") contained in the publications on our platform. However, Taylor & Francis, our agents, and our licensors make no representations or warranties whatsoever as to the accuracy, completeness, or suitability for any purpose of the Content. Any opinions and views expressed in this publication are the opinions and views of the authors, and are not the views of or endorsed by Taylor & Francis. The accuracy of the Content should not be relied upon and should be independently verified with primary sources of information. Taylor and Francis shall not be liable for any losses, actions, claims, proceedings, demands, costs, expenses, damages, and other liabilities whatsoever or howsoever caused arising directly or indirectly in connection with, in relation to or arising out of the use of the Content.

This article may be used for research, teaching, and private study purposes. Any substantial or systematic reproduction, redistribution, reselling, loan, sub-licensing, systematic supply, or distribution in any form to anyone is expressly forbidden. Terms & Conditions of access and use can be found at <http://www.tandfonline.com/page/terms-and-conditions>

RESEARCH ARTICLE

Quasi-2D and prewetting transitions of square-well fluids on a square-well substrate

Ashim K. Saha^a, Satya Pal Singh^a, Jayant K. Singh^{a*} and Sang Kyu Kwak^b

^aDepartment of Chemical Engineering, Indian Institute of Technology Kanpur, Kanpur, India 208016;

^bDivision of Chemical and Biomolecular Engineering, School of Chemical and Biomedical Engineering, Nanyang Technological University, Singapore 637459

(Received 15 April 2009; final version received 29 July 2009)

Molecular simulation methodologies are employed to study the first-order transition of variable square-well (SW) fluids on a wide range of weak attractive surfaces. Surface phase diagram of SW fluids of attractive well diameter $\lambda_{ff} = 1.5, 1.75, 2.0$ on a smooth, structureless surface modelled by a SW potential is reported via grand-canonical transition-matrix Monte Carlo (GC-TMMC) and histogram reweighting techniques. Fluids with $\lambda_{ff} = 1.5$ and 1.75 show quasi-2D vapour–liquid phase transition; on the other hand, prewetting transition is visible for a SW fluid with larger well-extent $\lambda_{ff} = 2.0$. The prewetting line, its length, and closeness to the bulk saturation curve are found to depend strongly on the nature of the fluid–fluid and fluid–wall interaction potentials. Boundary tension of surface coexistence films is calculated by two methods. First, the finite size scaling approach of Binder is used to evaluate the boundary tension via GC-TMMC. Second, the results of the boundary tension are verified by virtue of its relation to the pressure tensor components, which are calculated using a NVT-Monte Carlo approach. The results from the two methods are in good agreement. Boundary tension is found to increase with the increase in the wall–fluid interaction range for the quasi-2D system; conversely, boundary tension for thin–thick film, at prewetting transition, decreases with the increase in the wall–fluid interaction range.

Keywords: prewetting transition; boundary tension; Monte Carlo simulation; square-well fluid

1. Introduction

Wetting behaviour of fluid–solid interfaces is of practical interest to technologically important areas like adsorption and coating. Wetting of patterned surfaces by liquids plays a key role in the fields of nano-fluidics and biophysics. Knowing the importance of wetting phenomena it is surprising to find that surface driven phase transition was first found in 1977 independently by Cahn [1] and Ebner and Saam [2], who reported the transition between partial and complete wetting. Since then, many groups have been actively working to understand the molecular behaviour of fluids near the solid surfaces. Excellent reviews have come lately, which summarize the recent accomplishments in this field [3,4]. Wetting transition is associated with a temperature called wetting temperature, T_w . Above the wetting temperature one can observe thin and thick films in coexistence for pressures less than the bulk saturation pressure. Such a scenario is feasible for a suitable ratio and range of fluid–substrate interaction with respect to the fluid–fluid interaction. Interplay of these interactions can cause continuous growth of the thick film, referred to as the second-order transition, or the first-order

transition, known as the prewetting transition, where thin and thick films coexist. The prewetting transition line stems from the saturation curve at the wetting transition point, T_w , and terminates at the prewetting critical point, T_{pwc} , where thin and thick films become indistinguishable.

Since the seminal works of Ebner and Saam, and Cahn, the wetting transition has been observed experimentally for various surfaces, such as He on Cs [5,6], He on Rb [7] and K [8], and acetone on graphite [9]. Several theoretical [10–12] and simulation [13–18] approaches have been used to understand the wetting transition. In particular, argon on solid carbon-dioxide has been investigated by several investigators by various means [19–21]. There are other model systems, though, for which the prewetting transition has been observed [12,22–24]. The first Monte Carlo (MC) simulation on the prewetting transition was done by Finn and Monson on model argon on solid carbon-dioxide surface [14]. Subsequently, many different systems have been tried to investigate the prewetting and wetting transitions using Monte Carlo techniques [15,22,23]; in particular, extensive work has been done for simple gases on alkali metal surfaces by Curtarolo

*Corresponding author. Email: jayantks@iitk.ac.in

and co-workers [25–28]. In addition, Omata and Yonezawa [29] studied the effect of fluid–substrate interaction on the prewetting transition. In earlier work [18] we investigated the effect of strength of fluid–substrate interaction on the boundary tension of coexistence quasi-2D films on a substrate. While the majority of the work has been done on planar surfaces, Bohlen and Schoen [30] studied the prewetting transitions on nonplanar surfaces. In recent years with the development of advanced methodologies such as GC-TMMC [31], it is more feasible to investigate the first-order phase transition [32–34] including the prewetting transition, as shown by Errington and co-workers for model argon on solid carbon surface [16,17]. Compared with Monte Carlo techniques, molecular dynamics (MD) is less utilized to predict the prewetting transition; nonetheless in conjunction with Monte Carlo techniques; MD is very useful to predict boundary tension, as shown in previous work [18].

It was noted by a few authors that the interaction range can have a substantial effect on the wetting or drying transition [35,36]. Mean field theory indeed has predicted the dominant effect of long range forces on the surface phase transition [37]. This work is primarily to investigate the effect of fluid–wall interaction range on the behaviour of SW fluids of variable range using molecular simulation techniques. This paper mainly focuses on two aspects. First, we investigate the effect of attractive well width of fluid–fluid and wall–fluid interactions on the phase diagram and boundary tension of coexistence films, particularly from quasi-2D state to prewetting regime. Second, we investigate the performance of step function, [38] which has been used successfully for calculating pressure and interfacial properties of bulk fluid represented by discontinuous potential, with respect to GC-TMMC for the calculation of boundary tension. In order to understand the effect of range of attraction region on the first-order surface phase transition, the SW potential is chosen as it is one of the suitable choices. The SW potential is a popular model and is used by many researchers to study a range of model systems [32,33,38–41] including phase transitions near surfaces [18,42].

In this work, fluid–fluid interaction is modelled as SW potential, which is represented as:

$$u_{\text{ff}}(r_{ij}) = \begin{cases} \infty, & 0 < r_{ij} < \sigma_{\text{ff}} \\ -\varepsilon_{\text{ff}}, & \sigma_{\text{ff}} \leq r_{ij} < \lambda_{\text{ff}}\sigma_{\text{ff}} \\ 0, & \lambda_{\text{ff}}\sigma_{\text{ff}} \leq r_{ij} \end{cases} \quad (1)$$

where σ_{ff} , ε_{ff} and λ_{ff} are hard-sphere diameter, potential well depth, and well diameter of fluid–fluid

potential, respectively. The fluid–wall interaction is also modelled by the following SW type potential:

$$u_{\text{wf}}(z) = \begin{cases} \infty, & 0.8\sigma_{\text{ff}} > z \\ -\varepsilon_{\text{wf}}, & 0.8\sigma_{\text{ff}} \leq z < \lambda_{\text{wf}}\sigma_{\text{ff}} \\ 0, & \lambda_{\text{wf}}\sigma_{\text{ff}} \leq z \end{cases} \quad (2)$$

where ε_{wf} and λ_{wf} are corresponding parameters for fluid–substrate potential and z is the distance perpendicular from the surface. We have kept $0.8\sigma_{\text{ff}}$ as an effective hard-sphere diameter for the fluid–wall interaction, which is derived from the Argon–CO₂ interaction potential [14]. All variables reported in this study are reduced by ε_{ff} and σ_{ff} . For example, reduced temperature is given by $k_{\text{B}}T/\varepsilon_{\text{ff}}$, where k_{B} is the Boltzmann’s constant. Units are adopted such that σ_{ff} and ε_{ff} are unity.

The paper is organized as follows. Section 2 describes the simulation methods used in this study. Section 3 presents the results of phase-coexistence, density profile, and boundary tension of coexisting films with the variation of the strength of substrate potential and fluid–fluid potential. Section 4 concludes our study.

2. Methodologies

The phase diagram of a thin–thick film is calculated using a GC-TMMC simulation technique. The method is described in detail elsewhere [16,17], however, for the sake of completeness, we provide a brief description of the methodology. GC-TMMC simulations are conducted in a grand-canonical ensemble at constant chemical potential μ , volume V , and temperature T . Microstate probability in this ensemble is represented as

$$\pi_s = \frac{1}{\Xi} \frac{V^{N_s}}{\Lambda^{3N_s} N_s!} \exp[-\beta(U_s - \mu N_s)] \quad (3)$$

where $\beta = 1/k_{\text{B}}T$ is the inverse temperature, Ξ is the grand partition function, U_s denotes the interaction energy of particles of microstate s , is the de Broglie wavelength, and N_s stands for the number of particles.

In GC-TMMC simulations three basic Monte Carlo moves are used, namely displacement, insertion and deletion moves. During moves, attempted transitions between microstates of different densities are monitored. At regular intervals during a simulation, this information is used to obtain an estimate of the density probability distribution, which is subsequently used to bias the sampling to low probability densities using multi-canonical sampling [43]. Over time all densities of interest are sampled adequately. The final

result is an efficient self-adaptive method for determining the density probability distribution over a specified range of densities. Once a probability distribution has been collected at a given value of chemical potential, histogram reweighting [44] is used to shift the probability distribution to other values of the chemical potential. Coexistence chemical potential is calculated by histogram reweighting [44] until we obtain a probability distribution, Π_N^{coex} , such that areas under the thin and thick film regions in the probability distribution plot are equal. Densities of phases are calculated from the first moment of Π_N^{coex} distribution. Coexistence pressure is obtained using the following expression [16,17]:

$$\beta p V = \ln \left(\sum_N \Pi_N^{\text{coex}} / \Pi_0^{\text{coex}} \right) - \ln(2). \quad (4)$$

In addition to the calculation of coexistence pressures, densities, and energies, grand-canonical Monte Carlo simulation can also be combined with finite-size scaling methods to evaluate the boundary tension. This method does not require establishing and maintaining an interface, as would be the case for NVT ensemble simulation. The interfacial energy for a finite-size system with a substrate length of L is determined from the maximum likelihood in the thick film $\Pi_{\text{max}}^{\text{thick}}$ and thin film regions $\Pi_{\text{max}}^{\text{thin}}$ and minimum likelihood in the interface region Π_{min}

$$\beta F_L = \frac{1}{2} (\ln \Pi_{\text{max}}^{\text{thin}} + \ln \Pi_{\text{max}}^{\text{thick}}) - \ln \Pi_{\text{min}}. \quad (5)$$

The interfacial free-energy of thin–thick film on a two dimensional surface varies with the system size according to the Binder's formalism and is given by (see [17] for more detail)

$$\beta \tau_L = \frac{\beta F_L}{2L} = C_1 \frac{1}{L} + C_2 \frac{\ln(L)}{L} + \beta \tau \quad (6)$$

where τ_L is the interfacial tension for a system of box length L , τ is the boundary tension for infinite system, C_1 and C_2 are constants and F_L represents the free energy of the thin–thick interface for a finite system size L .

In this work, we have estimated the thin–thick film critical parameters by using the coexistence data and the least square fit of the following scaling law:

$$(N/A)_{\text{thick}} - (N/A)_{\text{thin}} = C \left(1 - \frac{T}{T_{\text{sc}}} \right)^{\beta_c} \quad (7)$$

where $(N/A)_{\text{thick}}$ and $(N/A)_{\text{thin}}$ are surface densities of thick and thin films, respectively and C and β_c are fitting parameters.

The surface critical temperature, T_{sc} , estimated from Equation (7) is used to calculate the critical density, $(N/A)_c$, from the least square fit of the following equation:

$$\frac{(N/A)_{\text{thick}} + (N/A)_{\text{thin}}}{2} = (N/A)_c + D(T - T_{\text{sc}}) \quad (8)$$

where D is a fitting parameter.

Scaling analysis as used in this work is an approximate method to obtain critical properties. For accurate values, finite size scaling analysis [45–47] is the most suitable method. However, we do not perform such rigorous analysis in this work.

To obtain the relation of boundary tension with pressure tensor components, we start with the fundamental relation of Helmholtz potential for a system of an inhomogeneous film on a substrate as would be the case for thin and thick films at coexistence on a substrate. The following relation holds for the infinitesimal and reversible transformation [48]:

$$dF = -S dT + \mu dN - P_{xx} s_y s_z ds_x - P_{yy} s_x s_z ds_y - P_{zz} s_x s_y ds_z \quad (9)$$

where F is the Helmholtz free energy, S is the entropy, N is the amount of the fluid, s_i is the thickness of the fluid in the direction of i , and P_{ii} is the ii th component of the pressure tensor.

In this work, we have placed a hard wall at a distance $s_z = H$ from the substrate of area $A = s_x s_y$. H is sufficiently large to have any noticeable effect on the fluids near the substrate. If the volume, V , of the simulation box is defined as $s_x s_y s_z$ and the total length of the thin–thick film interface $L_l = 2s_y$, then the above equation can be rewritten as follows:

$$dF = -S dT + \mu dN - P_{zz} dV - s_z (P_{xx} - P_{zz}) \times dA - \frac{s_x s_z}{2} (P_{yy} - P_{xx}) dL_l. \quad (10)$$

The above equation can be written in terms of work contribution due to various tensions [48]:

$$dF = -S dT + \mu dN + \gamma_1 dV + \gamma_2 dA + \tau dL_l, \quad (11)$$

where γ_1 , γ_2 and τ are various tension factors.

Comparing Equations (10) and (11), at a constant substrate area A , V , N and T , the boundary tension τ is expressed as follows:

$$\tau = \left(\frac{\partial F}{\partial L_l} \right)_{A,V,N,T} = \frac{s_x s_z}{2} (P_{xx} - P_{yy}). \quad (12)$$

In the current work, $s_z = H$, i.e. the distance between the substrate and the hard wall is kept constant, which

simplifies the above equation. Hence, the thin–thick boundary tension is given by

$$\tau = \frac{HL_x[P_{xx} - P_{yy}]}{2}, \quad (13)$$

where P_{xx} is the pressure tensor component in the x direction, which is perpendicular to the thin–thick film interface. P_{yy} is the pressure tensor component in the y direction, which is parallel to the thin–thick film interface. Pressure-tensor components are obtained using procedure described by Orea *et al.* [38]

2.1. Simulation details

The GC-TMMC simulation box was set up such that one side (bottom plane perpendicular to the z direction, see Figure 5) acted as a surface plane with attractive SW potential. The opposite side was chosen to be a repulsive wall to keep the fluid molecules inside the simulation box. The repulsive wall was kept at a height of 20 in the z direction (i.e. $L_z=20$) to avoid the effect of repulsive wall on the attractive surface. The other sides of the box, L_x and L_y , were equal in length. The lateral variation of the box in these two directions represents varied system sizes with surface areas of $L_x \times L_y$. Periodic boundary condition was applied only in x and y directions. Four independent runs were performed to calculate the statistical error.

In NVT-MC simulations, we start by placing the molecules on the attractive surface of the simulation box with $L_z=20$ such that initial surface density (number of molecules/surface area) is slightly higher than coexistence surface density of the thick film. The second step is to create a vacuum by expanding the simulation cell in the x direction such that $L_x=3*L_y$. Using the above geometry and initial set-up we performed NVT-MC simulations using 2000 particles. Eight million cycles were taken as equilibration period and an equal number for production cycles.

3. Results and discussion

3.1. Quasi-2D phase transition

We start our discussion with the adsorption isotherm of a SW fluid with $\lambda_{ff}=1.5$. Figure 1 presents the surface density as a function of chemical potential for various wall–fluid interaction values at a constant temperature $T=0.68$. We observed a discontinuity, in the isotherm, which is a characteristic feature of the first-order transition. Such surface phase transition is seen also for different wall–fluid interaction strengths [18]. The chemical potential corresponding to the surface phase transition decreases with the increasing

wall–fluid interaction range. Surface density gradually increases with increasing chemical potential beyond the surface phase transition value; and it eventually diverges as the chemical potential approaches the bulk saturation chemical potential. Figure 2 presents the adsorption isotherms for $\lambda_{ff}=1.5$ and $\lambda_{wf}=2.2$ at various temperatures. The behaviour seen for $\lambda_{ff}=1.5$ is akin to quasi-2D or prewetting transition. Since the prewetting transition is known to stem from the saturation curve at the wetting temperature, obtaining the wetting temperature is an important

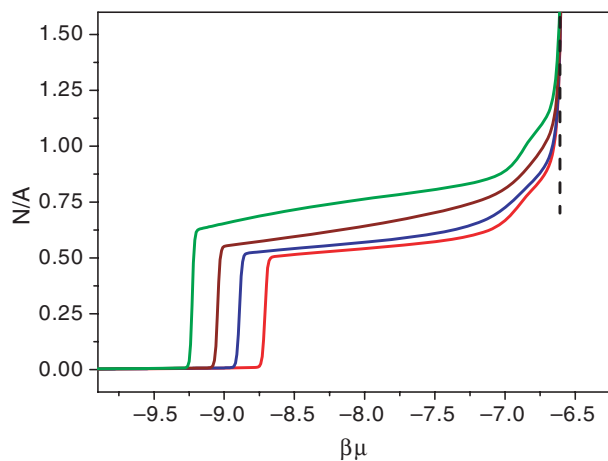


Figure 1. Adsorption isotherms of a SW fluid with $\lambda_{ff}=1.5$. Lines from left to right correspond to the wall–fluid interaction ranges, $\lambda_{wf}=2.8, 2.6, 2.4$ and 2.2 at $T=0.68$. The dashed line represents the bulk coexistence chemical potential.

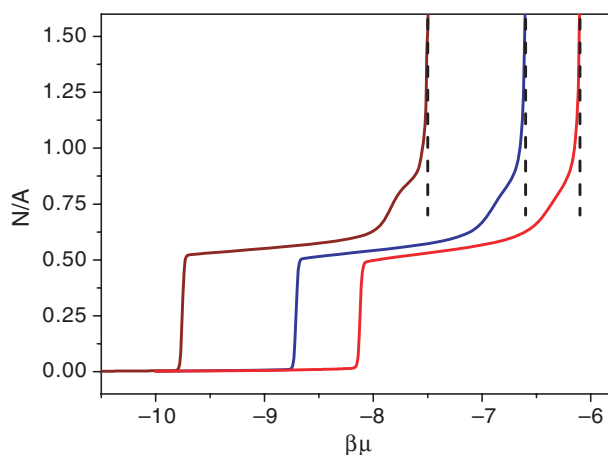


Figure 2. Adsorption isotherms of a SW fluid with $\lambda_{ff}=1.5$ and $\lambda_{wf}=2.2$. Lines from left to right correspond to the isotherms at $T=0.62, 0.68$ and 0.72 . Dashed lines represent the corresponding bulk coexistence chemical potential for different temperatures.

aspect to signify the prewetting transition. It is noted that as the temperature is decreased, the difference in the coexistence chemical potential for the surface phase transition and the bulk saturation chemical potential does not decrease for $\lambda_{ff}=1.5$ (Figure 3). On the contrary, a slight increase is noticed in the difference of the chemical potentials with decrease in the temperature. Similar behaviour is also observed for $\lambda_{ff}=1.75$ at different wall–fluid interaction ranges, which is contradictory to what is seen for the prewetting transitions [4]. Certainly, these observations suggest that the surface phase transition of SW fluids with relatively smaller interaction range is a quasi-2D vapour–liquid phase transition. This behaviour is also similar to the first layering transition observed for various other systems [49].

The phase coexistence envelopes of the quasi-2D vapour and liquid phases for $\lambda_{ff}=1.5$ and variable λ_{wf} are illustrated in Figure 4. At lower temperatures until $T=0.8$, the density of the quasi-2D vapour is insensitive to the change in the wall–fluid interaction range. Contrary to the quasi-2D vapour, the quasi-2D liquid is extremely sensitive to the variation in the wall–fluid interaction range. Even at a lower temperature increased λ_{wf} increases the density of the coexistence quasi-2D liquid phase. For example, at $T=0.62$, a 29% increase in the quasi-2D liquid density was observed with increase in λ_{wf} from 2.2 to 2.8; whereas, the change is suppressed at higher temperature, $T=0.8$, where the density increases by only 22%. The consequence of such an effect on the coexistence quasi-2D liquid film is seen on the surface critical density and critical temperature, which are found to

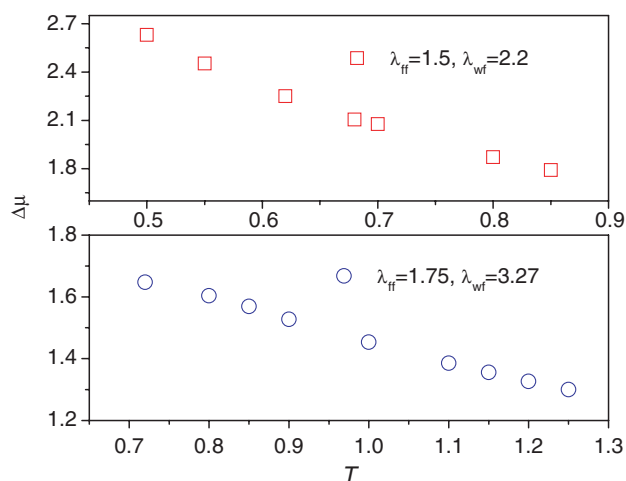


Figure 3. Difference in surface coexistence chemical potential and bulk saturation chemical potential as a function of temperature for $\lambda_{ff}=1.5$ and 1.75.

increase with increase in the wall–fluid interaction range. Critical temperature and density are calculated using Equations (7) and (8). Using least square fit of Equation (7), we obtained critical exponent, β_c , in the range of 0.175 to 0.2 for various wall–fluid interaction ranges studied in this work. The fitted value of β_c deviates from the 2D Ising model value of 1/8. This discrepancy is attributed to the system size effect. For example, increase in the number of particles from 700 to 1300, decreases β_c from 0.175 to 0.155. Hence, significant system size effect in the critical exponent is noted. On the other hand, the effect of system size on critical temperature and density is insignificant. Typical snapshots of the quasi-2D vapour–liquid configuration, obtained from NVT-MC simulations, are displayed in Figure 5. Similar phase coexistence behaviour is observed for higher fluid–fluid well-extent, $\lambda_{ff}=1.75$, as shown in Figure 6.

To understand structural changes due to increase in the wall–fluid interaction range, density profiles were obtained for coexistence quasi-2D vapour and liquid phases using the NVT-MC technique. Figure 7 presents the density profiles of two coexistence films. The density profiles show the interplay of wall–fluid and fluid–fluid interactions. In the case of the lower fluid–fluid interaction range $\lambda_{ff}=1.5$, two layers are clearly visible for $\lambda_{wf}=2.2$ as shown in Figure 7(a). The interaction range of fluid–substrate allows two layers of molecules within the well width. The number of molecules in the liquid like film increases with increasing well width of the surface field. A similar behaviour is also seen in Figure 4. Such enhancement in the number of molecules in the quasi-2D liquid-film

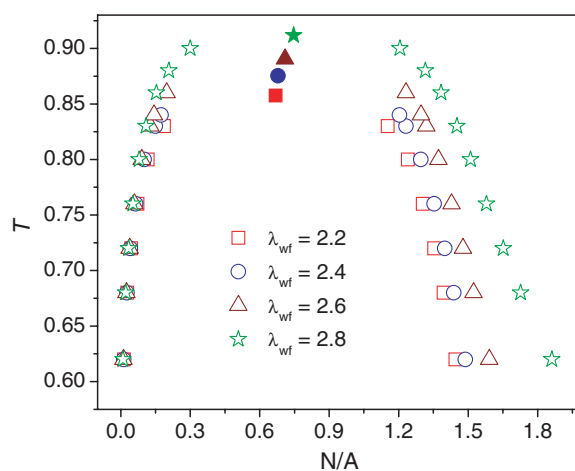


Figure 4. Quasi-2D vapour–liquid coexistence envelope of a SW fluid for wall–fluid interaction ranges, $\lambda_{wf}=2.2, 2.4, 2.6$ and 2.8 at a constant fluid–fluid well-extent, $\lambda_{ff}=1.5$. The estimated critical points are displayed by filled symbols.

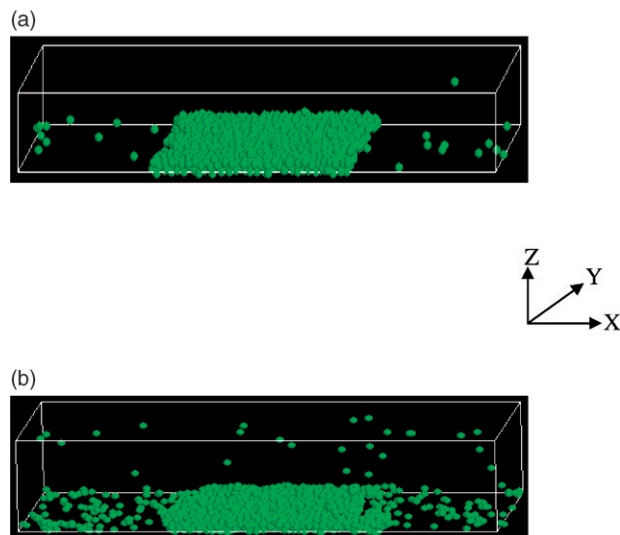


Figure 5. Typical quasi-2D phase separation of a SW fluid with $\lambda_{ff}=1.5$ and $\lambda_{wf}=2.2$. at (a) $T=0.62$ and (b) $T=0.8$.

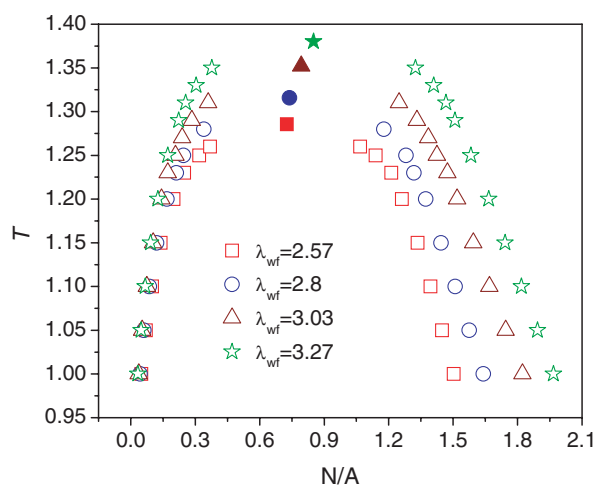


Figure 6. Quasi-2D vapour-liquid coexistence envelope of a SW fluid for wall-fluid interaction range, $\lambda_{wf}=2.57, 2.8, 3.03$ and 3.27 at a constant fluid-fluid well-extent, $\lambda_{ff}=1.75$. The estimated critical points are displayed by filled symbols.

led to the collection of molecules in another layer other than the existing two layers; as a result the profile shows small plateau near the edge of the first layer. Similar behaviour is seen for $\lambda_{wf}=2.4$ and 2.6 . Such rearrangements reduce the peak density of the existing layers for the intermediate wall-fluid well-extent compared to that of $\lambda_{wf}=2.2$. At the wall-fluid interaction range of 2.8 a small peak is distinctively observed, which indicates the formation of another molecular layer in the middle region of the well. The quasi-2D vapour film, however, does not bear the layering since a relatively larger surface is exposed to

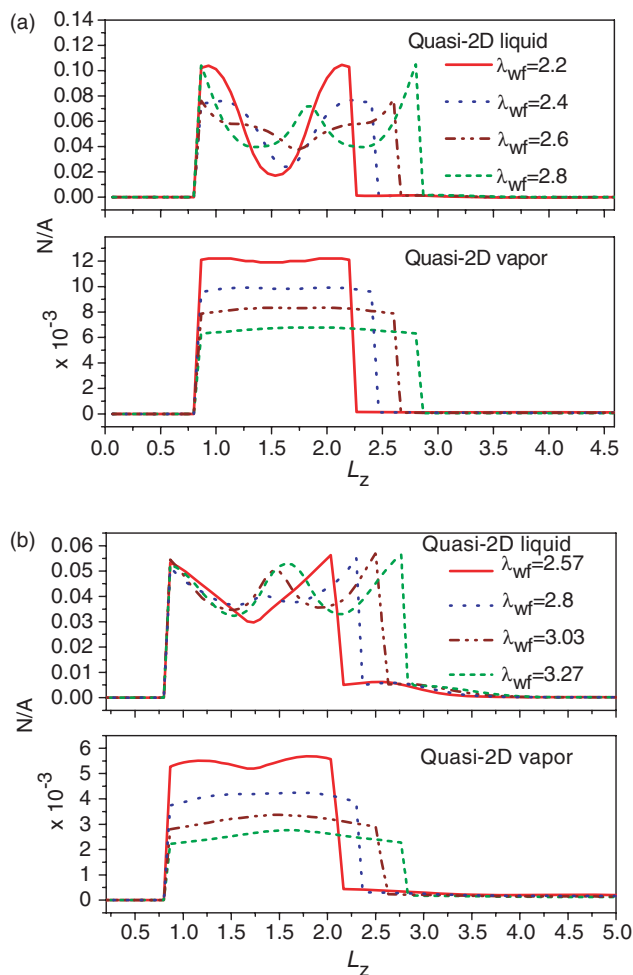


Figure 7. Density profile of quasi-2D vapour-liquid film for (a) $\lambda_{ff}=1.5$, $\lambda_{wf}=2.2, 2.4, 2.6$ and 2.8 at $T=0.68$; (b) $\lambda_{ff}=1.75$, $\lambda_{wf}=2.57, 2.8, 3.03$ and 3.27 at $T=1.2$.

the molecules in low number. Thus, hard core interactions of fluid-fluid molecules have less impact and the molecules tend to float uniformly within the wall-fluid well-extent.

For fluid-fluid well-extent, $\lambda_{ff}=1.75$, the V-shape trough, which is seen at $\lambda_{wf}=2.57$, depicts the separation of the two layers as shown in Figure 7(b); however it vanishes and a small peak appears at $\lambda_{wf}=2.8$. This is indicative of the formation of another layer in the middle of the existing two layers. The most interesting observation, which is in contrast to the case of $\lambda_{ff}=1.5$, is the accumulation of the molecules immediately outside the wall-fluid interaction range. This behaviour is completely missing for the shorter range fluid as seen in Figure 7(a). Such behaviour is not observed in the quasi-2D vapour phase; nevertheless, density is not as flat as observed for the case of $\lambda_{ff}=1.5$. In the middle of the well-width range,

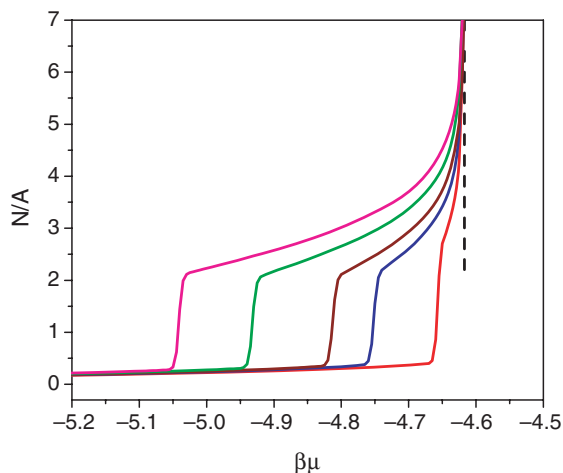


Figure 8. Adsorption isotherms of a SW fluid with $\lambda_{ff}=2.0$. Lines from left to right correspond to the wall–fluid interaction range, $\lambda_{wf}=3.47, 3.2, 2.93, 2.8$ and 2.6 at $T=1.9$. The dashed line represents the bulk saturation chemical potential.

depletion in the density of quasi-2D liquid phase at lower wall–fluid well-extent occurs.

In summary, the fluid–fluid attractive well-widths $\lambda_{ff}=1.5$ and 1.75 display quasi-2D behaviour although there is slight change in the nature of the behaviour in the presence of longer wall–fluid interaction. In subsequent section, we present the results for a SW fluid with a longer interaction range.

3.2. Prewetting transition

Figure 8 presents the adsorption isotherms for $\lambda_{ff}=2.0$, for various wall–fluid interaction ranges at a constant temperature. The behaviour is noticeably different from that of shorter interaction range SW fluids, where the effect of wall–fluid interaction range is not as drastic as seen for $\lambda_{ff}=2.0$. Surface phase transition is found missing for the wall–fluid interaction range less than 2.6 at $T=1.9$, as shown in the figure. The interesting aspect of the surface phase transition seen for $\lambda_{ff}=2.0$ is the closeness of the chemical potential, corresponding to the first-order transition, to the bulk saturation chemical potential with decrease in the wall–fluid interaction range. The effect of long range interaction, which is seen in the adsorption isotherms, is also seen on the density profiles of the coexistence films, as shown in Figure 9. The structure of the liquid-like film is skewed towards the end of the wall–fluid well-extent but also the heap outside the well-extent is intensified. A relatively higher accumulation of particles was seen near the end of wall–fluid interaction range mainly due

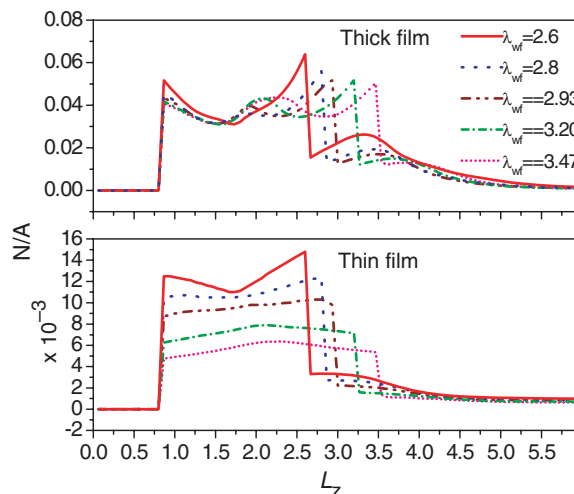


Figure 9. Density profile of thin–thick film for $\lambda_{ff}=2.0$, $\lambda_{wf}=2.93, 3.2, 3.47$ and 3.73 at $T=1.98$.

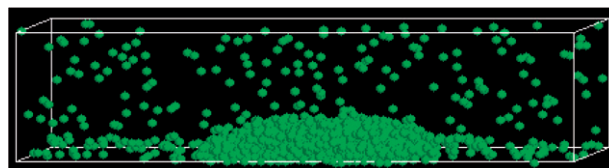


Figure 10. Typical phase separation of thin–thick film at $T=1.75$ for $\lambda_{ff}=2.0$ and $\lambda_{wf}=2.8$.

to the influence of the wall and the fluid molecules within the well-width on the molecules in the last layer within the wall–fluid well-extent. Such possibilities are partially missing for molecules in the first layer near the wall as fluid–fluid interactions are relatively fewer compared to molecules near the end of the wall–fluid well-extent. The thin film, on the other hand, does not exhibit significant structural variation within the range of wall–fluid interaction, although a small mound was observed immediately outside the wall–fluid interaction range, which is due to the same reason seen for the thick film. The growth of the layer beyond the wall–interaction range suggests a possible divergence below some lower temperature, which indicates the existence of prewetting transition instead of quasi-2D vapour–liquid transition. A typical snapshot of the configuration of the film for $\lambda_{ff}=2.0$ is given in Figure 10, which clearly shows the presence of the multi-layer liquid-like film, which is entirely different from that seen for $\lambda_{ff}=1.5$ and 1.75 .

To obtain a final confirmation of the prewetting transition, we calculated the difference between the thin–thick coexistence chemical potential and the bulk saturation value, for various temperatures, $\Delta\mu(T)$, and

extrapolated it to obtain the wetting temperature for which the above difference approaches zero. Figure 11 presents the scaling form of the above difference for various wall–fluid interaction ranges, which clearly indicates the presence of the prewetting transition for the longer fluid–fluid interaction range. Figure 12 presents a rigorous thin–thick film phase diagram of SW fluid of well-extent 2.0 on substrates of various wall–fluid interaction ranges. We do not perform the scaling analysis as done for quasi-2D system (see Equation (7)) to obtain the prewetting critical temperature, T_{pwc} . Instead, it is calculated by obtaining the free-energy barrier between the two coexisting

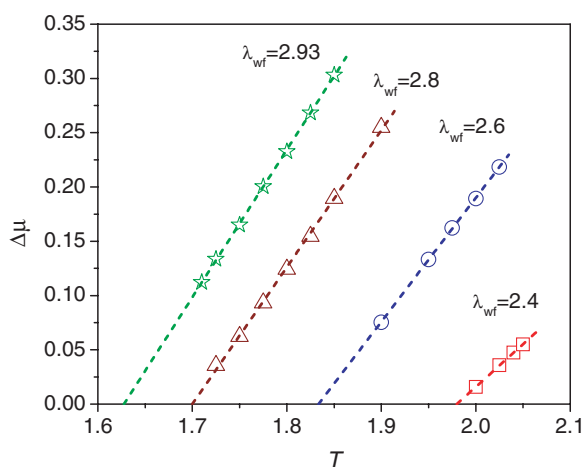


Figure 11. Temperature dependence of the difference between the bulk and prewetting saturation chemical potentials. The dashed lines represent extrapolation to the wetting temperature.

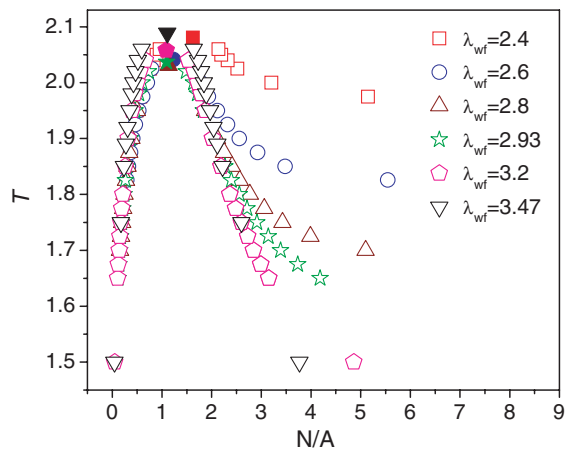


Figure 12. Thin–thick film coexistence envelopes of a SW fluid with well-extent, $\lambda_{\text{ff}}=2.0$, for wall–fluid interaction range, $\lambda_{\text{wf}}=2.4, 2.6, 2.8, 2.93, 3.2$ and 3.47 . The estimated critical points are displayed by filled symbols.

phases (see Figure 13) for various temperatures and extrapolating it to the temperature where it becomes zero.

Bonn and Ross [4] presented a generalized picture of the prewetting transition based on few experimental observations. Their study suggested the following form, which would in general provide estimates of the distance between the prewetting line and the bulk coexistence line:

$$-\Delta\mu(T)/k_{\text{B}}T_{\text{w}} \cong \alpha[(T - T_{\text{w}})/T_{\text{w}}]^{\beta}, \quad (14)$$

where, α and β are 0.5 and 1.5, as per Bonn and Ross's experimental observations. The above power law scaling exponent, $\beta=3/2$, has also been predicated theoretically by Schick and Taborek [50] for Lennard-Jones based substrate–fluid interaction: $u_{\text{wf}} \sim z^{-3}$. However, for short and finite range forces, thickness of the thick film varies differently compared to that seen for Lennard-Jones type forces [51]. Hence the above scaling form with $\beta=3/2$ does not hold for strictly finite range forces as used in the current study, which is also shown by Pandit and co-workers in their theoretical work [51].

Figure 14 presents the above scaling form for $\lambda_{\text{ff}}=2.0$ and variable wall–fluid interaction range. Interestingly, we did not observe a single curve for various wall–fluid interaction ranges contrary to the observation of Bonn and Ross though the variation is small. Moreover, the scaling exponent, β , and proportionality constant, α , for the current system are in the

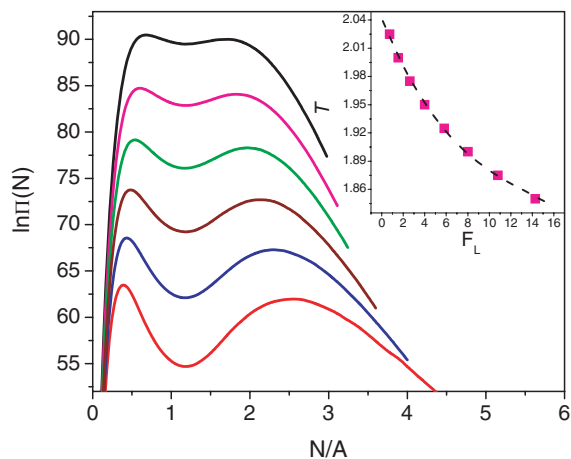


Figure 13. Coexistence surface density probability of thin–thick film for $\lambda_{\text{ff}}=2.0$ and $\lambda_{\text{wf}}=2.6$. The lines from the bottom are for the temperatures $T=1.9, 1.925, 1.95, 1.975, 2.0$ and 2.025 . Inset plot shows temperature vs. free energy barrier between thin and thick films. Symbols are the simulation data and the dashed curve represents extrapolation to the prewetting critical temperature.

range of $0.965 \sim 1.02$, and $0.8033 \sim 1.4477$, respectively. These values are considerably different from those found by Bonn and Ross, as expected. Further, Bonn and Ross observed $-\Delta\mu(T_{\text{pwc}})/T_w \cong 0.03$; however, for the current system we observed this value increase from 0.037 to 0.76, with an increase in the wall–fluid interaction range from 2.4 to 3.47. Surprising, a similar discrepancy was also observed by Seller and Errington for LJ based potential [52]. This study suggests that Ross and Bonn’s observation cannot be generalized for all combinations of fluid and substrate interactions since the prewetting line, its length and closeness to saturation curve depend strongly on the nature of the fluid–fluid and fluid–wall interaction potential.

Surface and prewetting critical temperatures for all the systems studied in this work including 2D and 3D bulk critical temperatures are listed in Table 1. The change in $T_{\text{sc}}/T_{\text{bc}}$, where T_{bc} is the bulk critical temperature, is linear with the increase in the well-extent ratio $\lambda_{\text{wf}}/\lambda_{\text{ff}}$. It is apparent that $T_{\text{sc}}/T_{\text{bc}}$ substantially varies depending on the fluid–fluid and substrate–fluid interaction range. On the other hand $T_{\text{pwc}}/T_{\text{bc}}$ appears to be confined in a narrow range. Interestingly, the ratio of surface critical temperature (including that of prewetting transition) and 2D critical temperature increases with the increasing fluid–fluid interaction range. In this work, T_{pwc}/T_c is found to vary from 0.758 to 0.779. These values are slightly higher than that of Ne–Mg (0.672) [25] and Ar–CO₂ (0.696) [16]. However, these values are smaller than that of Ne–CO₂ [53] for which T_{pwc}/T_c is 0.900. Surprisingly, T_{pwc}/T_c of water on graphite (0.775–0.783) predicted by Zhao [23] is very close to the higher end of T_{pwc}/T_c range in our work. On the other hand, the prewetting temperature ($T_{\text{pwc}}/T_c = 0.99$) of Hg on

sapphire [54] is extremely close to the bulk critical temperature.

3.3. Boundary tension of coexistence surface phases

One of the objectives of this work is to compare two methods; viz. GC-TMMC and NVT-MC along with step function technique [38], for the evaluation of the boundary tension of the surface coexistence phases. Binder’s formalism along with the GC-TMMC method is employed to calculate the boundary tension of the infinite system size from a set of finite system size calculations. Figure 15 presents the comparison of the boundary tension calculated from the GC-TMMC and the NVT-MC for varied wall–fluid interaction ranges at different temperatures. The results via the two methods are in good agreement. Errors are in the range of $1 \sim 2\%$ in GC-TMMC, whereas they are found to be $8 \sim 15\%$ in NVT-MC simulations. Therefore, GC-TMMC seemingly is a better choice for the investigation of wetting transitions. Particularly, the ability to use multi-processors to fill the transition matrix in a disjoint fashion is an appealing feature of the method, especially for the calculation of boundary tension of

Table 1. Critical temperature and density of quasi-2D and prewetting transitions of SW fluids for various wall–fluid interaction ranges from GC-TMMC simulations. Bulk 3D and 2D critical temperature, T_{bc} , and $T_c(2D)$, respectively, are taken from the literature. The error in the surface critical temperature and surface density represent one standard deviation of the mean for four independent runs.

	T_{bc} [32]	$T_c(2D)$ [56]	λ_{wf}	T_{sc}	$(N/A)_{\text{sc}}$
$\lambda_{\text{ff}} = 1.5$	1.2172(7)	0.5609(3)	2.2	0.858(3)	0.668(2)
			2.4	0.875(2)	0.679(2)
			2.6	0.891(3)	0.709(1)
			2.8	0.912(2)	0.747(2)
$\lambda_{\text{ff}} = 1.75$	1.809(2)	0.7065(1)	2.57	1.285(1)	0.726(2)
			2.8	1.316(9)	0.738(3)
			3.03	1.352(6)	0.794(2)
			3.27	1.381(4)	0.851(2)
	T_{bc} [32]	$T_c(2D)$ [56]	λ_{wf}	T_{pwc}	$(N/A)_{\text{pwc}}$
$\lambda_{\text{ff}} = 2.0$	2.68(1)	0.9132(4)	2.4	2.081(8)	1.622(6)
			2.6	2.042(9)	1.231(8)
			2.8	2.031(7)	1.134(6)
			2.93	2.037(4)	1.094(5)
			3.20	2.058(3)	1.089(5)
			3.47	2.089(3)	1.109(2)
			3.73	2.131(8)	1.133(4)

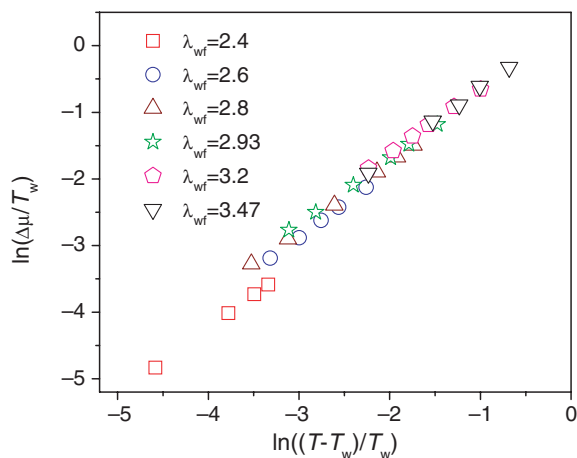


Figure 14. Scaled prewetting phase diagram for $\lambda_{\text{ff}} = 2.0$.

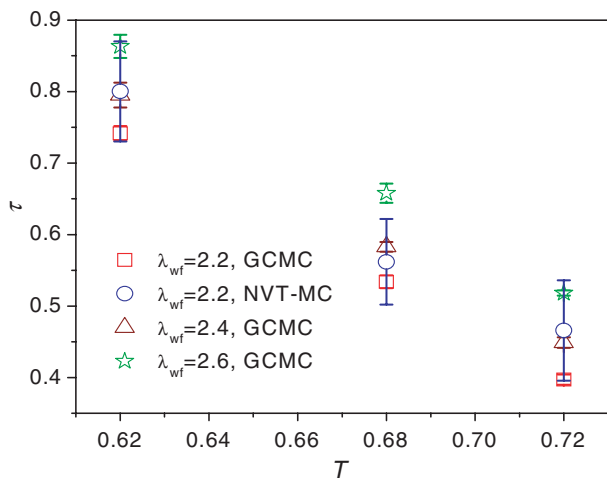


Figure 15. Boundary tension as a function of temperature for $\lambda_{ff}=1.5$ and $\lambda_{wf}=2.2, 2.4$ and 2.6 at temperatures, $T=0.62, 0.68$ and 0.72 .

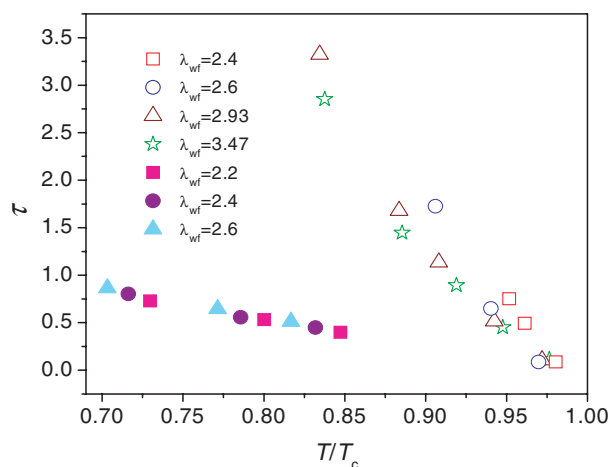


Figure 16. Boundary tension of SW fluids of different wall–fluid interaction range versus temperature in the reduced form, obtained from GC-TMMC and finite size scaling techniques. T_c is the surface or prewetting critical temperature for quasi-2D or prewetting transition, respectively. Open and filled symbols represent $\lambda_{ff}=2.0$ and $\lambda_{ff}=1.5$, respectively.

simple fluids. However, GC-TMMC’s performance is yet to be seen for more complex systems such as acetone on a graphite surface [9]. Figure 15 also presents the effect of wall–fluid interaction range on the boundary tension of the quasi-2D film. Increased wall–fluid interaction range is found to increase the boundary tension of the quasi-2D vapour–liquid coexistence film. Boundary tension is found to be linear with the temperature, for the range of temperature studied in this work. Interestingly, the effect of wall–fluid interaction on the boundary tension of SW fluid with

$\lambda_{ff}=2.0$ is clearly different from that of the quasi-2D system seen in Figure 16, which presents a comparison of boundary tensions for quasi-2D and prewetting systems. Increased wall–fluid interaction is found to decrease the boundary tension of thin–thick film. Boundary tension between quasi-2D films is extremely small compared to that for thin–thick film at a prewetting condition. Further, any effect of wall–fluid interaction range on quasi-2D tension is eliminated under the reduced temperature condition, which is evident from Figure 16. As expected the boundary tension decreases with increasing temperature and eventually approaches zero at the surface critical temperature. This is analogous to the behaviour of bulk vapour–liquid surface tension [24]. Boundary tension values can be used in the form of Guggenheim scaling relation $\tau = \tau_0(1 - \frac{T}{T_c})^r$ to understand the corresponding states behaviour of quasi-2D and prewetting transition systems. It is well known that the critical exponent, r , is 1.0 for the 2D Ising model [55]. We expect that all the systems studied in this work have 2D Ising model-like behaviour. For quasi-2D SW based systems we found exponent r falls in the range 1.06–1.1, which is reasonably close to the value of the 2D Ising model. On the other hand, for prewetting transitions, the exponent at lower wall–fluid interaction range is 2.4. We found, however, that r increases first and subsequently decreases with increasing wall–fluid interaction range with $r=1.63$ at $\lambda_{wf}=3.47$. The critical exponent related to boundary tension for the prewetting transition of finite range potential differs substantially from that of the 2D-Ising model, which is contrary to expectations. We do not know the reason for such deviation of prewetting SW systems from the true 2D Ising model system. A more detailed analysis on the critical exponent for finite range forces would be helpful, and we plan to study this in the near future.

4. Conclusions

Two methodologies are utilized to calculate the boundary tension between two films, at coexistence, on a smooth structure-less substrate. GC-TMMC is used to obtain the phase coexistence values of the thin–thick film. GC-TMMC requires multiple simulations to get the infinite size boundary tension; however, it is the preferred method in the vicinity of the critical temperature. Although NVT-MC along with step function to calculate the pressure tensor components is also a useful method, for simple fluids GC-TMMC is relatively superior. While the work has been limited to the simple systems bearing no direct resemblance to

any experimental situations, the results provide detailed insights into the wetting behaviour of model fluids near a solid surface. The interesting finding is the quantitative evidence of the sensitivity of the surface phase transition to the interaction ranges of fluid–fluid and wall–fluid. Prewetting transition is found to occur for longer fluid–fluid interaction ranges. On the other hand the quasi-2D vapour–liquid transition is prevalent for short interaction range fluids. The boundary tension increases with the increase in the wall–fluid interaction range for the quasi-2D system, but boundary tension for thin–thick film, at prewetting transition, decreases with the increase in the wall–fluid interaction range. Our analysis, similar to that of Bonn and Ross, suggests that a corresponding state form $-\Delta\mu_{pw}(T)/k_B T_w \cong \alpha[(T - T_w)/T_w]^\beta$ is, in general, valid for various fluids with α and β dependent on the interaction potential form.

Acknowledgements

This work was supported by the Department of Science and Technology, Government of India (Grant Nos. SR/S3/CE10/2006 and IR/S3/EU/005/2007).

References

- [1] J.W. Cahn, *J. Chem. Phys.* **66**, 3667 (1977).
- [2] C. Ebner and W.F. Saam, *Phys. Rev. Lett.* **38**, 1486 (1977).
- [3] L.D. Gelb, K.E. Gubbins, R. Radhakrishnan, and M.S. Bartkowiak, *Rep. Prog. Phys.* **62**, 1573 (1999).
- [4] D. Bonn and D. Ross, *Rep. Prog. Phys.* **64**, 1085 (2001).
- [5] J.E. Rutledge and P. Taborek, *Phys. Rev. Lett.* **69**, 937 (1992).
- [6] R.B. Hallock, *J. Low Temp. Phys.* **101**, 31 (1995).
- [7] J.A. Phillips, D. Ross, P. Taborek, and J.E. Rutledge, *Phys. Rev. B* **58**, 3361 (1998).
- [8] J.A. Phillips, P. Taborek, and J.E. Rutledge, *J. Low Temp. Phys.* **113**, 829 (1998).
- [9] F. Kruchten and K. Knorr, *Phys. Rev. Lett.* **91**, 085502 (2003).
- [10] E. Cheng, M.W. Cole, W.F. Saam, and J. Treiner, *Phys. Rev. Lett.* **67**, 1007 (1991).
- [11] F. Ancilotto and F. Toigo, *Phys. Rev. B* **60**, 9019 (1999).
- [12] S.M. Gatica, J.K. Johnson, X.C. Zhao, and M.W. Cole, *J. Phys. Chem. B* **108**, 11704 (2004).
- [13] S. Ebner and W.F. Saam, *Phys. Rev. B* **35**, 1822 (1987).
- [14] J.E. Finn and P.A. Monson, *Phys. Rev. A* **39**, 6402 (1989).
- [15] J.E. Finn and P.A. Monson, *J. Chem. Phys.* **99**, 6897 (1993).
- [16] J.R. Errington, *Langmuir*. **20**, 3798 (2004).
- [17] J.R. Errington and D.W. Wilbert, *Phys. Rev. Lett.* **95**, 226107 (2005).
- [18] J.K. Singh, G. Sarma, and S.K. Kwak, *J. Chem. Phys.* **128**, 044708 (2008).
- [19] S. Sokolowski and J. Fischer, *J. Phys. Rev. A* **41**, 6866 (1990).
- [20] R. Evans and P. Tarazona, *Phys. Rev. A* **28**, 1864 (1983).
- [21] W. Shi, X. Zhao, and J. Johnson, *Mol. Phys.* **100**, 2139 (2002).
- [22] B.M. Malo, A. Huerta, O. Pizio, and S. Sokolowski, *J. Phys. Chem. B* **104**, 7756 (2000).
- [23] X. Zhao, *Phys. Rev. B* **76**, 041402 (2007).
- [24] S. Saquin and M. Schoen, *J. Chem. Phys.* **118**, 1453 (2003).
- [25] M.J. Bojan, G. Stan, S. Curtarolo, W.A. Steele, and M.W. Cole, *Phys. Rev. E* **59**, 864 (1999).
- [26] S. Curtarolo, G. Stan, M.W. Cole, M.J. Bojan, and W.A. Steele, *Phys. Rev. E* **59**, 4402 (1999).
- [27] S. Curtarolo, G. Stan, M.J. Bojan, M.W. Cole, and W.A. Steele, *Phys. Rev. E* **61**, 1670 (2000).
- [28] S. Curtarolo, M.W. Cole, and R.D. Diehl, *Phys. Rev. B* **70**, 115403 (2004).
- [29] K. Omata and F. Yonezawa, *J. Phys. Condens. Matter*. **10**, 9431 (1998).
- [30] H. Bohlen and M. Schoen, *J. Chem. Phys.* **120**, 6691 (2004).
- [31] J.R. Errington, *J. Chem. Phys.* **118**, 9915 (2003).
- [32] J.K. Singh, D.A. Kofke, and J.R. Errington, *J. Chem. Phys.* **119**, 3405 (2003).
- [33] J.K. Singh and D.A. Kofke, *J. Chem. Phys.* **121**, 9574 (2004).
- [34] S.K. Kwak, J.K. Singh, and J. Adhikari, *Chemical Product and Process Modeling* **2**, 8 (2007).
- [35] M.J.P. Nijmeijer, C. Bruin, A.F. Bakker, and J.M.J. van Leeuwen, *J. Phys. Condens. Matter*. **4**, 15 (1992).
- [36] S. Dietrich, in *Phase Transitions and Critical Phenomena*, edited by C. Domb and J. Lebowitch (Academic, London, 1988).
- [37] S. Dietrich and M. Napiorkowski, *Phys. Rev. A* **43**, 1861 (1991).
- [38] P. Orea, Y. Duda, and J. Alejandre, *J. Chem. Phys.* **118**, 5635 (2003).
- [39] J.K. Singh and S.K. Kwak, *J. Chem. Phys.* **126**, 024702 (2007).
- [40] J.K. Singh and D.A. Kofke, *Mol. Sim.* **30**, 343 (2004).
- [41] J. Alejandre, Y. Duda, and S. Sokolowski, *J. Chem. Phys.* **118**, 329 (2003).
- [42] F. van Swol and J.R. Henderson, *J. Chem. Soc. Faraday Trans. II* **82**, 1685 (1986).
- [43] B.A. Berg and T. Neuhaus, *Phys. Rev. Lett.* **61**, 9 (1992).
- [44] A.M. Ferrenberg and R.H. Swendsen, *Phys. Rev. Lett.* **61**, 2635 (1988).
- [45] A.D. Bruce and N.B. Wilding, *Phys. Rev. Lett.* **68**, 193 (1992).
- [46] N.B. Wilding, *J. Phys. Condens. Matter*. **9**, 585 (1997).
- [47] D. Nicolaides and R. Evans, *Phys. Rev. Lett.* **63**, 778 (1989).
- [48] M. Schoen and D.J. Diestler, *Phys. Rev. E* **56**, 4427 (1997).

- [49] I. Brovchenko and A. Oleinikova, *Interfacial and Confined Water* (Elsevier, Amsterdam, 2008).
- [50] M. Schick and P. Taborek, *Phys. Rev. B* **46**, 7312 (1992).
- [51] R. Pandit, M. Schick, and M. Wortis, *Phys. Rev. B* **26**, 5112 (1982).
- [52] M.S. Sellers and J.R. Errington, *J. Phys. Chem. C* **112**, 12905 (2008).
- [53] F. Ancilotto and F. Toigo, *J. Chem. Phys.* **112**, 4768 (2000).
- [54] Y. Ohmura, Y. Kajihara, and M. Yao, *Phys. Rev. E* **63**, 051601 (2001).
- [55] R.K. Pathria, *Statistical Mechanics* (Elsevier, Oxford, 1996).
- [56] S. Jana, J.K. Singh, and S.K. Kwak, *J. Chem. Phys.* **130**, 214707 (2009).